In vitro reconstitution of Sgk3 activation by phosphatidylinositol-3-phosphate

Daniel Pokorny[1,2], Linda Truebestein[1,2], Kaelin D. Fleming[3], John E. Burke[3,4] and Thomas A. Leonard[1,2,5*]

[1]Department of Structural and Computational Biology, Max Perutz Labs, Campus Vienna Biocenter 5, 1030 Vienna, Austria

[2]Department of Medical Biochemistry, Medical University of Vienna, 1090 Vienna, Austria

[3]Department of Biochemistry and Microbiology, University of Victoria, Victoria, BC, Canada V8W 2Y2

[4]Department of Biochemistry and Molecular Biology, The University of British Columbia, Vancouver, British Columbia V6T 1Z3, Canada

[5]Correspondence: thomas.leonard@meduniwien.ac.at

Summary

Serum- and glucocorticoid-regulated kinase 3 (Sgk3) is activated by the phospholipid phosphatidylinositol-3-phosphate (PI3P) downstream of growth factor signaling and by Vps34-mediated PI3P production on endosomes. Upregulation of Sgk3 activity has recently been linked to a number of human cancers. Here, we show that Sgk3 is regulated by a combination of phosphorylation and allosteric activation by PI3P. We demonstrate that PI3P binding induces large conformational changes in Sgk3 associated with its activation, and that the PI3P binding pocket of the PX domain of Sgk3 is sequestered in its inactive conformation. Finally, we reconstituted Sgk3 activation via Vps34-mediated PI3P synthesis on phosphatidylinositol liposomes *in vitro*. In addition to defining the mechanism of Sgk3 activation by PI3P, our findings open up potential therapeutic avenues in allosteric inhibitor development to target Sgk3 in cancer.

31 **Introduction**

32 Cellular membranes are hotspots at which numerous signaling pathways controlling
33 various aspects of cell physiology and pathology converge. One of the most
34 intensively studied pathways downstream of extracellular growth factors is the
35 phosphoinositide 3-kinase (PI3K) pathway. PI3K activation by receptor tyrosine
36 kinases, G-protein-coupled receptors, or RAS leads to the generation of various
37 phosphoinositide lipids, that serve as a platform for the recruitment and activation of
38 effector molecules (Martini *et al*, 2014). Dysregulation of PI3K signaling is frequently
39 observed in cancer, diabetes, neurodegenerative and cardiac disorders, and other
40 diseases (Fruman & Rommel, 2014; Fruman *et al*, 2017), making the pathway a
41 prominent target for pharmacological inhibition (Marone *et al*, 2008).

42 Many important downstream effectors of PI3K are protein kinases. Protein
43 phosphorylation is a ubiquitous post-translational modification that regulates cell
44 signaling and is carried out by the arsenal of more than 500 protein kinases in the
45 human proteome (Manning, 2002). Since the mechanism of phosphotransfer
46 catalyzed by protein kinases is highly conserved (Endicott *et al*, 2012), individual
47 kinases have evolved unique regulatory mechanisms to ensure that they can faithfully
48 respond to different, often very transient, lipid-based signaling cues (Leonard &
49 Hurley, 2011).

50 Serum- and glucocorticoid-regulated kinase 3 (Sgk3) [also known as cytokine-
51 independent survival kinase (CISK)] is a serine/threonine protein kinase that is
52 activated downstream of growth factors (Liu *et al*, 2000). Like the closely related

53 kinase Akt, it belongs to the AGC kinase family and is activated by phosphorylation of
54 a hydrophobic motif in its C-terminal tail by mTORC2 (Bago *et al*, 2016) and
55 subsequent PDK1-dependent phosphorylation of its activation loop (Kobayashi &
56 Cohen, 1999; Kobayashi *et al*, 1999). A third site, called the turn motif, also in the tail,
57 regulates the stability of Akt and protein kinase C (PKC) (Ikenoue *et al*, 2008;
58 Facchinetti *et al*, 2008), but its phosphorylation has not been reported in Sgk3.
59 Distinct from the activation of Akt by PIP_3 or $PI(3,4)P_2$, Sgk3 depends on the lipid
60 phosphatidylinositol-3-phosphate (PI3P) for its activation (Virbasius *et al*, 2001).
61 Sgk3 is recruited specifically to endosomes via its PI3P-binding phox homology (PX)
62 domain (Tessier & Woodgett, 2006; Xing *et al*, 2004), which promotes
63 phosphorylation of its activation loop and hydrophobic motif by PDK1 and mTORC2
64 respectively (Tessier & Woodgett, 2006; Bago *et al*, 2014, 2016). Two major pathways
65 drive the production of PI3P on endosomes: downstream of phosphatidylinositol-
66 3,4,5-trisphosphate (PIP_3) production by class I PI3K at the plasma membrane,
67 phosphatidylinositol-3,4-bisphosphate [$PI(3,4)P_2$] is produced by the action of SH2-
68 containing inositol 5' phosphatase (SHIP2) (Liu *et al*, 2018; Goulden *et al*, 2019).
69 Phosphatidylinositol-3-phosphate (PI3P) is generated either from $PI(3,4)P_2$ by
70 inositol polyphosphate 4-phosphatases (INPP4) (Ivetac *et al*, 2005) or, de novo, from
71 phosphatidylinositol by the class III PI3K Vps34 (Backer, 2008). Both pathways have
72 been shown to contribute to Sgk3 activation (Bago *et al*, 2014; Malik *et al*, 2018).

73 Sgk isoforms are transcriptionally induced by serum and glucocorticoid
74 hormones (Webster *et al*, 1993) and are involved, among others, in the regulation of
75 ion channels, transcription factors, enzymatic activities and have been implicated in

76 hair growth defects and renal dysfunction (Lang *et al*, 2006). Recently, Sgk3 has been
77 shown to play a role in different cancers in an Akt-independent manner (Gasser *et al*,
78 2014; Bago *et al*, 2016; Vasudevan *et al*, 2009; Wang *et al*, 2017), highlighting the
79 importance of Sgk3 as an effector downstream of PI3K signaling. Despite its
80 physiological and pathological relevance, however, relatively little is known about the
81 precise mechanism of Sgk3 regulation. In this manuscript, we provide clear evidence
82 for the allosteric activation of Sgk3 by PI3P, highlighting the role of the PX domain
83 and PI3P in the regulation of Sgk3 enzymatic activity. Our findings have obvious
84 implications for the spatial and temporal control of Sgk3 activity as well as for the
85 design of Sgk3-targeted therapeutics.

86

87 **Results**

88 **Sgk3 localizes specifically to PI3P-containing endosomes**

89 The Sgk3 PX domain (residues 1-124) has previously been shown to bind to PI3P, and
90 is required for localization at early endosomes (Xu *et al*, 2001; Chandra *et al*, 2019;
91 Virbasius *et al*, 2001; Bago *et al*, 2014). Serum-starved HeLa cells transfected with
92 mCherry-Sgk3 show a punctate endosomal membrane localization (Fig. 1A), which is
93 lost upon 20 min treatment with the PI3K inhibitor wortmannin (Fig. 1B). The
94 membrane localization of Sgk3 is strictly dependent on its PX domain, since a binding
95 site mutant of Sgk3 ($Sgk3^{R90A}$) fails to localize to endosomes in the same cells (Fig. 1C-
96 D). This is further illustrated by a representative cross section intensity profile (Fig.
97 1E-F). These data confirm both the specificity of Sgk3 for PI3P *in vivo* and the
98 endosomal localization of Sgk3 to endosomes.

99

100 ***In vitro* characterization of recombinant Sgk3**

101 The phosphorylation state of recombinant human Sgk3 co-expressed with PDK1 and
102 purified from baculovirus-infected insect cells was characterized by tandem mass
103 spectrometry (Supplementary Figure 1A). Sub-stoichiometric (~20%) activation
104 loop (Thr320) phosphorylation was observed; however, phosphorylated peptides
105 were not observed for either the turn motif (Ser461) or the hydrophobic motif
106 (Ser486), despite purification with phosphatase inhibitors known to preserve
107 phosphorylation at these sites in Akt1 (manuscript in revision). Turn motif
108 phosphorylation has previously been reported for Sgk1 (Chen *et al*, 2009) and other

109 AGC kinases, in particular Akt and PKC, in which it plays an important role in
110 regulating protein stability and degradation (Oh *et al*, 2010; Facchinetti *et al*, 2008;
111 Ikenoue *et al*, 2008; Hauge *et al*, 2007). Since both the turn motif and the basic patch
112 to which it binds on the kinase domain are conserved, it seemed logical to assume
113 that Sgk3 should also be modified at this site. Insects, however, do not express an
114 obvious homolog of Sgk3, raising the possibility that the kinase responsible for turn
115 motif phosphorylation of Sgk3 is also not present in insect cells. We therefore
116 expressed human Sgk3 in HEK293 cells and characterized its phosphorylation state
117 by tandem mass spectrometry. Surprisingly, phosphorylated peptides were again not
118 observed for either the turn motif or hydrophobic motif (Supplementary Figure 1B).
119 It is therefore an open question as to whether Sgk3 is indeed modified on the turn
120 motif and under what cellular conditions.

121 To prepare site-specifically phosphorylated Sgk3 for in vitro kinase assays,
122 both wild-type Sgk3 ($Sgk3^{WT}$) and kinase-dead Sgk3 ($Sgk3^{D286A}$) were
123 dephosphorylated with lambda phosphatase and re-phosphorylated with
124 recombinant PDK1. Specific modification of Sgk3 with a single phosphate on its
125 activation loop (Thr320) was confirmed by mass spectrometry (Supplementary
126 Figure 1C-D). The purification of recombinant Sgk3 was challenging, due to solubility
127 issues under certain purification conditions. However, careful optimization of the
128 purification protocol enabled us to purify Sgk3 in a detergent-free buffer with pH and
129 ionic strength, close to physiological values (see Materials and Methods). We
130 performed size-exclusion chromatography coupled to multi-angle light scattering to
131 determine its precise mass and monodispersity. Sgk3 exhibited a single peak with a

132 measured mass of 57.3 kDa, in close agreement with its actual mass reported by mass
133 spectrometry and a polydispersity value of 1.001 (Supplementary Figure 1E). To
134 ensure that the Sgk3 used in subsequent assays was monodisperse and remained so
135 for the duration of the assays, we measured the particle size distribution of Sgk3 by
136 dynamic light scattering at 0 and 60 min post-freeze-thaw under kinase assay buffer
137 conditions. Sgk3 exhibited near identical mass distributions centered around a
138 particle size of 3 nm at 0 and 60 min at 20°C (Supplementary Figure 1F).

139

140 **Sgk3 is specifically and allosterically activated by PI3P**

141 Previous studies have shown that loss of PI3P binding decreases phosphorylation of
142 Sgk3 on its activation loop and hydrophobic motif (Tessier & Woodgett, 2006), as well
143 as downstream substrate phosphorylation (Bago *et al*, 2016). However, it is not
144 known whether PI3P binding serves to allosterically activate Sgk3 in addition to its
145 known role in promoting phosphorylation of the activation loop and hydrophobic
146 motif (Bago *et al*, 2014). Previous studies have established that the closely-related
147 kinase Akt depends on the binding of PI(3,4,5)P_3 or PI(3,4)P_2 for full activity (Ebner
148 *et al*, 2017; Lučić *et al*, 2018). We therefore investigated whether PI3P is simply a
149 membrane anchor to target Sgk3 to endosomes, or whether PI3P also allosterically
150 governs Sgk3 activity.

151 Having established that our recombinant Sgk3 is well-behaved during our
152 assays, we assessed the influence of PI3P on kinase activity. Dephosphorylated Sgk3
153 exhibited undetectable kinase activity in vitro and could not be stimulated with PI3P

154 (Supplementary Figure 1G). To test whether PI3P allosterically activates Sgk3, we
155 bound PDK1-phosphorylated Sgk3^{WT} to liposomes with increasing PI3P
156 concentrations and assayed its kinase activity against Crosstide, a glycogen synthase
157 kinase 3β (GSK3β)-derived peptide substrate of Sgk3 (Dai *et al*), using a radiometric
158 kinase assay (Hastie *et al*, 2006). We observed robust, PI3P-dependent activation of
159 Sgk3, which correlated with the fraction of protein bound to the liposomes (Fig. 2A).
160 Both the activity and binding curves can be fitted with a one site binding model
161 characterized by nearly identical binding affinities of 24.6±10.8 μM and 29.3±8.0 μM,
162 respectively. No signal was observed in the control without Crosstide, thereby ruling
163 out autophosphorylation of Sgk3. Basal kinase activity against Crosstide seen in the
164 absence of PI3P can be explained by the high degree of activation loop
165 phosphorylation (Fig. S1C). To confirm that the observed activity comes exclusively
166 from Sgk3, we mutated D286 in the catalytic loop to alanine to create a kinase-dead
167 Sgk3. While this protein shows almost identical PI3P binding to Sgk3^{WT}, neither basal
168 nor PI3P-stimulated Crosstide phosphorylation was observed (Fig. 2B).

169 We next reconstituted Sgk3 activation by PI3P in vitro using a coupled Vps34-
170 Sgk3 kinase activity assay. Vps34 is the only class III PI3K expressed in mammalian
171 cells and generates PI3P from PI on endosomes and other endomembrane structures,
172 including autophagosomes (Hurley & Young, 2017; Backer, 2016). We prepared
173 liposomes containing 10 mol % PI as a substrate for Vps34 and monitored both Vps34
174 and Sgk3 activity simultaneously in a radiometric kinase assay (Fig. 2C). We could
175 detect a time-dependent production of PI3P in the liposomes and the consequent
176 activation of Sgk3 as a function of increasing PI3P (Fig. 2D). This demonstrates that

177 Sgk3 is allosterically activated by the product of class III PI3K activity, highlighting
178 that full Sgk3 activity requires membranes enriched in PI3P.

179

180 **HDX-MS reveals conformational changes in Sgk3 upon membrane binding**

181 Having demonstrated that Sgk3 is allosterically activated by PI3P, we next set out to
182 investigate the structural basis of PI3P-mediated activation. In previous studies on
183 Akt, we have shown that PI(3,4,5)P_3 or PI(3,4)P_2 binding relieves pleckstrin
184 homology (PH) domain-induced steric occlusion of the kinase domain catalytic cleft,
185 leading to Akt activation (Ebner *et al*, 2017; Lučić *et al*, 2018). To verify whether this
186 is also the case for Sgk3, we performed hydrogen-deuterium exchange mass
187 spectrometry (HDX-MS) on full-length Sgk3 and Sgk3 PX domain in the presence of
188 vesicles containing 0 or 5 mol % PI3P. Binding of the isolated PX domain to PI3P
189 vesicles led to dramatically lower exchange rates for peptides across the domain,
190 including the PI3P binding site, indicating that PI3P binding is captured by HDX-MS
191 analysis (Fig. 3A). We next compared the HDX rates between full-length $Sgk3^{WT}$ and
192 the isolated PX domain to determine whether they interact with each other. We
193 observed dramatic deprotection of the PX domain in the absence of the kinase domain
194 of Sgk3 (Fig. 3B), indicating that the PX domain is sequestered in an intramolecular
195 interaction in the full-length protein. Finally, we monitored HDX changes in full-
196 length Sgk3 upon PI3P binding. Protection of the PX domain upon membrane binding
197 was also observed, accompanied by deprotection in several areas of the kinase
198 domain. These sites form a contiguous network starting with β5, β7 and β8 strands

199 in the N-lobe and propagating to the C-lobe via the αG and αI helices (Fig. 3C).
200 Additional deprotection was observed in residues 468-476 localized in the C-terminal
201 tail. It was not possible to delineate a clear surface of interaction between the PX and
202 kinase domains from the changes in exchange rates in the kinase domain, but the data,
203 taken together, provide unambiguous evidence for an intramolecular PX-kinase
204 domain interaction and a large conformational change upon PI3P binding.

205

206 **Autoinhibition of Sgk3 impairs binding to PI3P**

207 Many AGC kinases that are activated by lipid second messengers exhibit a closed
208 conformation of their autoinhibited state in which the binding site for the lipid
209 headgroup is sequestered in an intramolecular interaction. To investigate whether
210 the autoinhibited conformation of Sgk3 might also sequester the PI3P-binding site of
211 its PX domain in intramolecular contacts, we compared the binding affinity for PI3P-
212 containing liposomes of full-length Sgk3 and its isolated PX domain. To ensure
213 identical conditions, we incubated both proteins with PI3P liposomes in a single
214 reaction, pelleted the liposomes, resolved the proteins in the supernatant and pellet
215 fraction by SDS-PAGE, and quantified their abundance by Coomassie stain
216 densitometry. To compensate for the lower staining sensitivity of the PX domain, we
217 used an N-terminally FITC-labelled version of this construct and quantified its
218 fluorescence intensity in the gel before Coomassie staining. We observed an
219 approximately 5-fold higher affinity to PI3P of the isolated PX domain over the full-

220 length protein (Fig. 4A), confirming that the PI3P binding site is sequestered by the
221 kinase domain in the autoinhibited state.

222 To substantiate this finding in vivo, we expressed mCherry-Sgk3^{WT} and eGFP-
223 Sgk3^{PX} in HeLa cells and imaged their localization in serum-starved cells by confocal
224 microscopy. While serum starvation of the cells overnight did not reduce PI3P levels
225 sufficiently to dissociate Sgk3 from endosomes (Fig. 1A), it was clear that the isolated
226 Sgk3 PX domain associates almost exclusively with endosomes (Fig. 4B), while full-
227 length Sgk3 exhibits a predominantly cytosolic distribution (Fig. 4C). A
228 representative cross-section intensity trace for both channels reveals that the bulk of
229 full length Sgk3 is uniformly distributed in the cytoplasm of cells, while the PX domain
230 is exclusively found on endosomes (Figure 4D-E). These findings confirm that the
231 PI3P binding pocket is sequestered in the autoinhibited conformation of Sgk3.

232

233 **Discussion**

234 Sgk3 is dependent on both PI3P and phosphorylation for its activity. We have shown
235 here that Sgk3 exhibits negligible activity in the absence of activation loop
236 phosphorylation and that PI3P significantly increases the basal activity of pre-
237 phosphorylated Sgk3. Like other AGC kinases regulated by phospholipids, including
238 Akt and PKC, the PI3P binding pocket of the PX domain of Sgk3 is sequestered in an
239 autoinhibitory, intramolecular conformation. This both necessitates PI3P for activity
240 and simultaneously raises the threshold level of PI3P that must be reached in the cell
241 in order to activate Sgk3. The structure of Akt1 reveals an intramolecular interaction

242 between its PH and kinase domains that obscures the PIP_3 binding site (manuscript
243 in revision), a feature which impairs its binding to PIP_3 in vitro and in vivo (Ebner *et*
244 *al*, 2017). Similarly, the diacylglycerol (DAG) binding site of the C1b domain of PKCβII
245 is also blocked by intramolecular contacts that impair its membrane translocation in
246 response to phorbol ester treatment (Leonard *et al*, 2011). More generally, the
247 regulatory C1 domains of all PKC isozymes, as well as those of the PKD family, are
248 engaged in autoinhibitory intramolecular interactions that impair their binding to
249 membranes (Oancea & Meyer, 1998; Lučić *et al*, 2016; Elsner *et al*, 2019).
250 Mechanistically, Sgk3 exhibits many of the features previously described for Akt,
251 though given the structural divergence between the PX domain of Sgk3 and the PH
252 domain of Akt, the atomistic details of autoinhibition are likely to be different. Sgk3 is
253 the only Sgk to comprise a full PX domain, although Sgk1 has been shown to possess
254 a short 'PX-like' domain in its N-terminus that mediates lipid binding (Pao *et al*, 2007).
255 Importantly, activation loop phosphorylation by PDK1 is insufficient to override the
256 requirement for PI3P for full Sgk3 activity, a property also shared by Akt (manuscript
257 in revision).

258 Whilst not the major focus of this study, it is worth noting that turn motif
259 phosphorylation of Sgk3 could not be observed in Sgk3 expressed either in insect or
260 human cells. This finding was unexpected, given the prominent role of turn motif
261 phosphorylation in other AGC kinases. Phosphorylation of the turn motif helps to
262 anchor the C-terminal tail of the kinase domain and increase the affinity of the
263 phosphorylated hydrophobic motif to its cognate hydrophobic pocket in the N-lobe
264 via local concentration, which leads to the overall stabilization of the kinase fold

265 (Hauge *et al*, 2007). While turn motif phosphorylation has been reported in all PKC
266 isoforms, Akt, Sgk1, and PKN (Hornbeck *et al*, 2004), whether it plays a role in Sgk3
267 regulation will require further investigation. Finally, it should also be noted that while
268 hydrophobic motif phosphorylation has been reported to increase the catalytic
269 activity of Sgk3 (Bago *et al*, 2014), our study does not address its contribution to Sgk3
270 activation.

271 Evidence suggests that PI3P binding by Sgk3 also promotes PDK1-dependent
272 phosphorylation of its activation loop. This mechanism of activation loop exposure
273 upon membrane binding is well established for Akt (Alessi *et al*, 1997; Stokoe *et al*,
274 1997). The requirement of PI3P for Sgk3 activity is therefore three-fold: in the first
275 place, it is required to target Sgk3 to membranes where it can encounter active PDK1;
276 secondly, PI3P binding triggers a conformational change that renders it a substrate
277 for PDK1; thirdly, and importantly, it is required to prevent autoinhibition of the
278 kinase domain by the PX domain. Studies on Akt have also implicated ATP in
279 stabilizing a phosphatase-resistant conformation of the kinase domain (Lu *et al*, 2015;
280 Lin *et al*, 2012; Chan *et al*, 2011), a mechanism which we recently showed to be
281 dependent on binding to membrane-embedded PIP_3 (Lučić *et al*, 2018). While such a
282 mechanism has not been explicitly shown for Sgk3, the homology between the kinase
283 domains and the mechanisms by which Akt and Sgk3 are activated suggests that this
284 is also likely to be the case for Sgk3 bound to PI3P-rich endosomes.

285 Our findings suggest that PI3P and phosphorylation are both required for Sgk3
286 activity, which makes Sgk3 a coincidence detector of both PI3P and PI3K signaling.

287 According to this model, PI3P-decorated endosomes lacking PDK1 would not serve as
288 signaling hubs for Sgk3. In this respect, it is worth noting that PDK1 does not bind to,
289 nor can it be activated by, PI3P. PDK1 binds with almost equal affinity to both
290 PI(3,4,5)P_3 (1.6 nM) and PI(3,4)P_2 (5.2 nM) (Currie *et al*, 1999), which targets it to
291 both the plasma membrane, which is abundant in PIP_3, and endomembranes, which
292 are decorated with PI(3,4)P_2 and heavily implicated in Akt signaling (Liu *et al*, 2018;
293 Ebner *et al*, 2017; Schenck *et al*, 2008; Braccini *et al*, 2015). PI3P is generally not
294 observed at the plasma membrane. Presumably, PDK1 and Sgk3 cooperate to drive
295 Sgk3 signaling on endosomes containing both PI(3,4)P_2 and PI3P (Figure 5). Indeed,
296 PDK1 has also been reported to associate with endosomes dependent on Sgk3
297 hydrophobic motif phosphorylation, where it inhibits ligand-induced degradation of
298 the chemokine receptor CXCR4 (Slagsvold *et al*, 2006). Sgk3 activity could therefore
299 be restricted to a subpopulation of endosomes with a specific phosphoinositide
300 composition. Interestingly, a recent large scale analysis of human PX domains
301 revealed the presence of a secondary lipid binding site in the PX domain of Sgk3 which
302 exhibits low-affinity PI(3,4)P_2 binding (Chandra *et al*, 2019). The functional
303 importance of the second lipid-binding site is still unclear, though one could easily
304 imagine that it might serve to either fine-tune the lipid binding specificity or increase
305 binding affinity via an avidity effect (Carlton & Cullen, 2005).

306 A similar model for PI(3,4)P_2-driven Akt activity on endomembranes has
307 recently been proposed to explain the transduction of growth factor signaling by Akt
308 at subcellular locations distal to the plasma membrane. In this model, both PDK1 and
309 Akt are targeted to PI(3,4)P_2-containing endomembranes, where they cooperate to

310 drive Akt signaling in the interior of the cell. Quantitative lipid imaging has revealed
311 that endosomal pools of PI(3,4)P_2 are signaling hubs for Akt (Liu *et al*, 2018). Like
312 Sgk3, Akt activity depends strictly on phosphorylation and the binding of its PH
313 domain to either PIP_3 or PI(3,4)P_2, thereby confining its activity to membranes
314 enriched in these signaling lipids (Ebner *et al*, 2017; Lučić *et al*, 2018; Siess & Leonard,
315 2019).

316 Such a model of localized Sgk3 activity may provide an explanation for the
317 reported overlap in Akt and Sgk3 substrate specificity (Kobayashi *et al*, 1999; Tessier
318 & Woodgett, 2006; Brunet *et al*, 2001; Murray *et al*, 2005). Notwithstanding the
319 similarity in their kinase domains, it is clear that their activity profiles would overlap
320 in such a model, since the PI(3,4)P_2 that drives PDK1 and Akt activation must be
321 present in membranes that support PI3P- and PDK1-mediated Sgk3 activation.
322 Indeed, a recent phosphoproteomic study identified several Sgk3-specific substrates
323 localized on endosomes (Malik *et al*, 2019). The reported role of Sgk3 in driving
324 human cancers in the absence of Akt hyperactivation is then also reconcilable with
325 this model and reinforces the potential value of Sgk3 as a therapeutic target either as
326 a monotherapy or in combination with Akt inhibitors.

327 The chemical toolkit for Sgk3 inhibition is still limited due to similarities with
328 other AGC kinases, such as Akt, and indeed with Sgk1 and Sgk2. However, inhibitor
329 14h has been reported to target all three Sgk isoforms without inhibiting Akt (Bago
330 *et al*, 2016) and, more recently, an Sgk3-specific PROTAC degrader has been
331 described (Tovell *et al*, 2019). Much effort has been aimed at developing allosteric

332 inhibitors of Akt that specifically target the autoinhibited conformation of the kinase
333 (Wu *et al*, 2010; Lapierre *et al*, 2016; Weisner *et al*, 2019), although despite high oral
334 bioavailability and specificity, none have yet made it to phase III clinical trials (Landel
335 *et al*, 2020). Nevertheless, the identification of an autoinhibitory intramolecular
336 interface in Sgk3, analogous but not homologous to Akt, presents opportunities for
337 the development of Sgk3-specific inhibitors that may have clinical value in the
338 treatment of cancers in which Sgk3 signaling is observed to be upregulated. Such
339 studies will undoubtedly benefit from the high-resolution structure determination of
340 full-length, autoinhibited Sgk3.

341

342 **Acknowledgements**

343 Intact mass analyses and phosphorylation mapping experiments were performed by
344 Dorothea Anrather and Thomas Gossenreiter from the Mass Spectrometry Facility at
345 the Max Perutz Labs using instruments of the Vienna BioCenter Core Facilities
346 (VBCF). We thank Justyna Sawa-Makarska and Sascha Martens (Max Perutz Labs) for
347 their generous gift of baculovirus for the expression of the Vps34 complex. This work
348 was supported by the Austrian Science Fund (FWF) grants P28135, P30584 and
349 P33066 to T.L. L.T. was supported by a Hertha Firnberg Postdoctoral Fellowship from
350 the Austrian Science Fund (FWF T915). J.E.B. is supported by a Michael Smith
351 Foundation for Health Research (MSFHR) Scholar award (17686), and an operating
352 grant from the Cancer Research Society (CRS-24368).

353

354 **Author Contributions**

355 D.P. purified all proteins and performed all biochemical experiments. L.T. performed
356 all fluorescence microscopy experiments. K.F. and J.B. performed all HDX-MS
357 experiments and analyzed the corresponding data. T.L. conceived the project.

358

359 **Declaration of Interests**

360 The authors declare no competing interests.

361

362 **Materials and methods**

363

364 **Fluorescence microscopy**

365 For localization studies of SGK3 in live cells, HeLa cells were co-transfected with
366 mCherry-SGK3 (wt) and either eGFP-SGK3^{PX} (residues 1-124) or eGFP-SGK3^{R90A}. Cells
367 were transfected using Turbofect transfection reagent according to the
368 manufacturer's protocol. Cells were serum starved overnight and changed into HBSS
369 for live imaging. Images were acquired 24 hours after transfection on a Zeiss LSM710
370 or LSM 700 confocal microscope equipped with a Zeiss 63x oil immersion objective
371 (NA 1.4) and 488 and 561 nm lasers. Image processing and analysis were done using
372 ImageJ 1.51j. All adjustments were applied uniformly across the entire image; no
373 nonlinear adjustments were used.

374

375 **Protein expression and purification**

376 Sgk3 PX domain (residues 1-124) was cloned into pHis-parallel bacterial expression
377 vector and transformed into *E. c*oli BL21 STAR electrocompetent cells. For large-scale
378 expression, the cells were grown in LB medium containing 100 µg/ml ampicillin at
379 37°C/180 RPM shaking, until OD_{600} reached 0.6. The temperature was lowered to
380 20°C, expression was induced by the addition of 0.1 mM IPTG and cells were grown
381 overnight. Cells were harvested by centrifugation at 4000g/20 min, the pellet was
382 flash-frozen in LN2 and stored at -80°C for further use. Pellet corresponding to 1 l of

383 culture was resuspended in 100 ml PX lysis buffer: 50 mM Tris pH 7.5, 150 mM NaCl,
384 20 mM imidazole, 1% glycerol, 1 mM TCEP, 1 mM PMSF, 1 mM benzamidine
385 hydrochloride , 2 mM $MgCl_2$, 1x protease inhibitor cocktail (made in-house: 100 μM
386 bestatin, 14 μM E-64, 10 μM pepstatin A, and 1 μM phosphoramidon), 5 μl Denarase.
387 The cell suspension was sonicated on ice, spun at 38 724 g, 4°C for 30 min. The soluble
388 fraction was loaded on a HisTrap FF 5 ml column (Cytiva) equilibrated in NiA buffer:
389 50 mM Tris pH 7.5, 150 mM Nacl, 20 mM imidazole, 1% glycerol, 1 mM TCEP. The
390 column was washed with 20 column volumes (CVs) of NiA, 10 CVs of high salt wash
391 buffer (NiA + 500 mM NaCl), an additional 10 CVs of NiA, and the bound protein eluted
392 with 0.02-1 M imidazole gradient over 10 CVs. Fractions containing His-tagged PX
393 domain were pooled and diluted with SA buffer in (50 mM Hepes pH 8.0, 1% glycerol,
394 1 mM TCEP). The His tag was cleaved with TEV protease (made in-house) overnight
395 at 4°C. The cleaved protein was loaded on HiTrap SP HP 1 ml cation exchange column
396 (Cytiva) equilibrated in SA buffer. The column was washed with 10 CVs of SA and
397 eluted with a 0-1 M NaCl gradient over 20 CVs. Fractions containing the PX domain
398 were diluted with SA to adjust NaCl concentration to ~150 mM and were either used
399 for Sortase labeling (see below) or concentrated to 20 mg/ml, snap-frozen in LN2 and
400 stored at -80°C for further use.

401 Purified PX domain was specifically labeled on its N-terminal glycine with a
402 FITC-LPETGG peptide (Genscript) in a Sortase-mediated reaction according to the
403 protocol described in (Theile *et al*, 2013). Briefly, the PX domain was incubated with
404 a 10-fold excess of FITC-LPETGG peptide in the presence of His-tagged Sortase A
405 (prepared in-house) and 5 mM $CaCl_2$ at 4°C overnight. Sortase was removed by NiNTA

406 affinity chromatography and the labeled PX domain purified from free label by size
407 exclusion chromatography on a Superdex 75 10/300 column equilibrated in 20 mM
408 Tris pH 8, 150 mM NaCl, 1% glycerol, 20 mM imidazole, 1 mM TCEP. Fractions
409 containing FITC-labeled PX domain were pooled, concentrated to 0.8 mg/ml, snap-
410 frozen in LN2 and stored at -80°C.

411 The human Sgk3 gene was codon optimized for expression in insect cells
412 (Genscript) and fused to the C-terminus of His_{10}/StrepII-tagged eGFP (A206K
413 monomeric variant) to aid expression of soluble Sgk3. Both wild-type and kinase-
414 dead (D286A) Sgk3 were expressed in baculvirus-infected Sf9 insect cells grown in
415 ESF 921 medium (Expression Systems) at 27°C. Cells were harvested 4-5 days post-
416 infection. Wild-type and D286A constructs were purified under identical conditions.
417 Briefly, the pellet of 0.5 l Sf9 cells was resuspended in 50 ml Sgk3 lysis buffer: 50 mM
418 Hepes pH 7.4, 50 mM NaCl, 1% glycerol, 1 mM TCEP, 1 mM PMSF, 1 mM benzamidine,
419 1 mM $MnCl_2$, 0.5 mM EDTA, 1x protease inhibitor cocktail, 0.1% CHAPS, 5 ul Denarase,
420 10 mM DTT, 1x protease inhibitor cocktail, 5 µl Denarase, 80 nM lambda phosphatase
421 (made in-house). The lysate was passed through Dounce homogenizer several times
422 and spun at 38 724 g (18 000 RPM), 4°C for 30 min. The soluble fraction was loaded
423 onto a StrepTrap HP 5 ml column (Cytiva) equilibrated in 50 mM Hepes 7.4, 50 mM
424 NaCl, 1% glycerol, 1 mM TCEP. The column was washed with 10 CVs of binding buffer
425 and the protein eluted with 2.5 mM *d*-desthiobiotin in binding buffer. Fractions
426 containing EGFP-Sgk3 were pooled and dephosphorylated with lambda phosphatase
427 in 50 mM Hepes pH 7.4, 150 mM NaCl, 1% glycerol, 10 mM DTT, 1 mM $MnCl_2$, 0.5 mM
428 EDTA, 0.5 µM lambda phosphatase (made in-house). Dephosphorylation was carried

429 out for 30 min at room temperature and 4°C overnight together with TEV cleavage of
430 the His/StrepII tag. To separate His-tagged lambda phosphatase from Sgk3, the
431 reaction mixture was loaded on HisTrap FF 1 ml column equilibrated in 20 mM Tris
432 pH 7.4, 150 mM NaCl, 1% glycerol, 1 mM TCEP. Dephosphorylated and cleaved Sgk3
433 was washed from the column with 20 mM imidazole, while lambda phosphatase
434 remained bound. Sgk3 was then site-specifically in vitro re-phosphorylated by GST-
435 PDK1 under the following conditions: 50 mM Tris pH 7.4, 150 mM NaCl, 1% glycerol,
436 1 mM TCEP, 1 mM ATP, 2 mM $MgSO_4$, 1:10 PDK1:Sgk3. The reaction was carried out
437 at 4°C for 3 h, then stopped by addition of 10 mM EDTA. GST-PDK1 was separated by
438 addition of glutathione-sepharose 4B beads (Cytiva) and incubation at 4°C overnight
439 with gentle rotation. Supernatant containing rephosphorylated Sgk3 was
440 concentrated in 30 kDa MWCO spin concentrator and injected onto Superdex 200
441 Increase 10/300 GL column (Cytiva) equilibrated in 20 mM Tris pH 7.4, 150 mM NaCl,
442 1% glycerol, 1 mM TCEP. Fractions containing Sgk3 were pooled, concentrated, snap-
443 frozen in LN2 and stored at -80°C for further use.

444 Recombinant baculovirus encoding Vps34 complex I (Atg6, protein A-tagged
445 Atg14, Vps15 and Vps34) (Sawa-Makarska *et al*, 2020) was used to infect 3 l of Sf9
446 insect cell culture. Cells were harvested 4-5 days post-infection. Pellets were lysed in
447 300 ml of Vps34 lysis buffer: 50 mM Tris pH 8.8, 300 mM Nacl, 1 mM DTT, 0.5 %
448 CHAPS, 1 mM $MgCl_2$, 0.5 mM PMSF, 1x protease inhibitor cocktail, 15 ul Denarase. The
449 lysate was passed several times through a Dounce homogenizer and spun at 38 724 g
450 (18 000 RPM), 4°C for 30 min. The soluble fraction was bound to IgG-Sepharose beads
451 (Cytiva) for 1 h at 4°C with gentle rotation. Resin was collected in a gravity flow

452 column and washed 3 x 50 ml wash buffer 1 (50 mM Tris pH 8, 300 mM NaCl, 1 mM
453 DTT, 0.5% CHAPS, 0.5 mM PMSF), 2 x 50 ml wash buffer 2 (50 mM Tris pH 8, 300 mM
454 NaCl, 1 mM DT, 2% glycerol, 0.25 % CHAPS). Finally, beads were resuspended in wash
455 buffer 2 and bound protein complex cleaved with TEV at 4°C overnight. The
456 supernatant containing the full Vps34 complex was concentrated and injected onto a
457 Superdex 200 Increase 10/300 GL column equilibrated in 50 mM Tris pH 8, 150 mM
458 NaCl, 1 mM TCEP, 2% glycerol. Fractions containing the complete complex of Atg6,
459 Atg14, Vps15 and Vps34 were pooled, concentrated to 0.9 mg/ml, snap-frozen in LN2
460 and stored at -80°C for further use.

461

462 **Intact mass spectrometry**

463 Intact protein samples were diluted in H_2O and up to 100 ng protein were loaded on
464 an XBridge Protein BEH C4 column (2.5 µm particle size, dimensions 2.1 mm X 150
465 mm; Waters) using a Dionex Ultimate 3000 HPLC system (Thermo Fisher Scientific)
466 with a working temperature of 50 °C, 0.1% formic acid (FA) as solvent A, 80%
467 acetonitrile, 0.08% FA as solvent B. Proteins were separated with a 6 min step
468 gradient from 10 to 80% solvent B at a flow rate of 300 µL/min and analysed on a
469 Synapt G2-Si coupled via a ZSpray ESI source (Waters). Data were recorded with
470 MassLynx V 4.1 (Waters) and analyzed using the MaxEnt 1 process to reconstruct
471 the uncharged average protein mass.

472

473 **Tandem mass spectrometry**

474 The reduced protein was denatured in 4 M urea, 50 mM ammonium bicarbonate
475 (ABC) and alkylated with 20 mM iodoacetamide for 30 min at room temperature in
476 the dark. The sample was diluted with 50 mM ABC down to 0.5 M urea and then
477 digested overnight using sequencing-grade endoproteinase GluC (Roche) at 25 °C.
478 The digestion was stopped by adding trifluoroacetic acid to a final concentration of
479 1% and the peptides were desalted using custom-made C18 stagetips (Rappsilber *et*
480 *al*, 2007). The peptides were separated on an Ultimate 3000 RSLC nano-flow
481 chromatography system (Thermo Fisher Scientific), using a pre-column for sample
482 loading (PepMapAcclaim C18, 2 cm × 0.1 mm, 5 µm) and a C18 analytical column
483 (PepMapAcclaim C18, 50 cm × 0.75 mm, 2 µm, both Dionex-Thermo Fisher Scientific),
484 applying a linear gradient from 2 to 35% solvent B (80% acetonitrile, 0.08% FA acid;
485 solvent A: 0.1% FA) at a flow rate of 230 nl/min over 60 min. Eluting peptides were
486 analysed on a Q Exactive HF or HF-X Orbitrap mass spectrometer equipped with a
487 Proxeon nanospray source (Thermo Fisher Scientific), operated in data-dependent
488 mode. Survey scans were obtained in a scan range of 375–1500 m/z, at a resolution
489 of 60000 at 200 m/z and an AGC target value of 3E6. The 8 most intense ions were
490 selected with an isolation width of 1.6 Da, fragmented in the HCD cell at 28% collision
491 energy and the spectra recorded at a target value of 1E5 and a resolution of 30000.
492 Peptides with a charge of +1 were excluded from fragmentation, the peptide match
493 and exclude isotope features were enabled and selected precursors were dynamically
494 excluded from repeated sampling. Raw data were processed using the MaxQuant
495 software package (version 1.6.0.16, http://www.maxquant.org/) (Cox & Mann, 2008)
496 and searched against a custom database containing the sequences of the Sgk3

497 constructs in the protein background of the expression system (either Spodoptera
498 spp. protein sequences available in Uniprot plus the Bombyx mori reference
499 proteome (www.uniprot.org) or the human proteome) plus the sequences of common
500 contaminants. The search was performed with full trypsin specificity and a maximum
501 of two missed cleavages, C-terminal cleavage to glutamate and aspartate for the GluC
502 digests or unspecific cleavage for pepsin digests. Carbamidomethylation of cysteine
503 residues was set as fixed, oxidation of methionine, protein N-terminal acetylation and
504 phosphorylation of serine, threonine and tyrosine as variable modifications—all
505 other parameters were set to default. Results were filtered at a false discovery rate of
506 10% at the peptide and protein level. Spectra of phosphorylated Sgk3 peptides were
507 validated manually. All proteomics data have been deposited in the PRIDE repository
508 (Perez-Riverol *et al*, 2019).

509

510 **Size exclusion chromatography with multiangle light scattering (SEC-MALS)**

511 80 µl of Sgk3 at 0.9 mg/ml was injected onto Superdex 200 Increase 10/300 GL
512 column (Cytiva) equilibrated in 20 mM Tris pH 8, 150 mM NaCl, 1% glycerol, 1 mM
513 TCEP. Separation was carried out using HPLC Agilent Technologies 1260 infinity with
514 a flow rate of 0.5 ml/min operated at room temperature. On-line light scattering of
515 690 nm laser was recorded on a miniDawn Treos detector (Wyatt Technology Corp.).
516 Shodex RI-101 (Shodex) refractive index detector was used to measure protein
517 concentration on-line. Data was analyzed using the ASTRA software (Wyatt
518 Technology Corp.).

519

520 **Dynamic light scattering (DLS)**

521 Autocorrelation curves of freshly thawed and centrifuged 7.5 μM Sgk3 in buffer
522 containing 20 mM Hepes pH 7.4, 150 mM NaCl, 1 % glycerol, 1 mM TCEP, 1 mM ATP,
523 2 mM $MgCl_2$, 100 μM Crosstide were recorded at 0 and 60 min of incubation at room
524 temperature. Measurements were performed on a DynaPro NanoStar instrument
525 (Wyatt Technology Corp.). Each measurement is an average of 10 acquisitions of 10 s
526 each.

527

528 **Sucrose-loaded vesicles (SLVs)**

529 Cholesterol, DOPC, DOPE, DOPS and liver PI were dissolved in chloroform, PI3P di C16
530 was dissolved in chloroform:methanol:water 1:2:0.8, PI(4,5)P_2 was dissolved in
531 chloroform:methanol:water 20:13:3. For liposomes with synthetic PI3P the lipids
532 were mixed in the following molar ratio: 20% cholesterol, 30 % DOPC, 15% DOPS,
533 35% DOPE. For liposomes containing PI3P, DOPC was substituted with 0-4% PI3P.
534 Liver PI liposomes contained 10% PI at the expense of DOPC. Lipid mixtures in
535 borosilicate glass tubes were evaporated with nitrogen to form a thin film and then
536 rehydrated by vortexing for 1 min with sucrose buffer (20 mM Hepes pH 7.4, 300 mM
537 sucrose). Resuspended lipids were subjected to 4 cycles of freezing in LN2 and
538 thawing in a sonicator bath. One volume of gel filtration buffer was added and
539 liposomes were pelleted in Beckman Coulter Optima MAX-XP Ultracentrifuge in TLA
540 100 rotor operated at 50 000 rpm/20°C for 30 min. The supernatant was discarded,

541 liposome pellets were resuspended in gel filtration buffer to a final lipid
542 concentration of 1 mM and stored for a maximum of two days at 4°C before use.

543

544 **Radiometric kinase assays**

545 Sgk3 kinase activity was monitored as the incorporation of radioactive phosphate
546 from γ^{32}P-ATP (Hartmann Analytic) into Crosstide (GRPRTSSFAEG), a validated Sgk3
547 substrate peptide. Sgk3 was mixed with PI3P-containing liposomes and incubated for
548 30 min at RT. 5 µl of liposomes-Sgk3 mixture was added to 5 ul of substrate master
549 mix to obtain following conditions: 20 mM Tris pH 8, 150 mM NaCl, 1% glycerol, 1
550 mM TCEP, 50 nM Sgk3, 100 µM Crosstide, 1 mM ATP (spiked 1:10 with γ^{32}P-ATP), 2
551 mM $MgCl_2$. The reaction was left to proceed for 15 min at room temperature and
552 stopped by addition of 2 µl of 0.5 M EDTA. 10 ul of the reaction was then spotted onto
553 a nitrocellulose membrane (0.2 um pore size), washed 5 x 3 min with 75 mM H_3PO_4
554 and the washed membrane inserted into a 20 ml polyethylene scintillation vial
555 containing 5 ml deionized H_2O. Cerenkov radiation was measured in a Tri-Carb 4910
556 TR liquid scintillator (Perkin Elmer). Datapoints were fitted with Michaelis-Menten
557 equation modified with a constant to reflect the basal enzymatic activity in 0% PI3P
558 condition:

559 $$V = \frac{V_{max}[PI3P]}{k_1 + [PI3P]} + const$$

560

561 **Liposome pelleting assay**

562 1 μM $Sgk3^{WT}$ or $Sgk3^{PX}$ was mixed 1:1 with liposomes, incubated at 20°C for 30 min
563 and spun at 9800g for 30 min at 20°C. Supernatant was collected and the liposome
564 pellet resuspended in gel filtration buffer. Equal volumes of supernatant and pellet
565 fractions were separated by SDS-PAGE and quantified by Coomassie densitometry. In
566 the comparative binding assay with full-length Sgk3 and $Sgk3^{PX}$ in the same reaction,
567 FITC-labelled PX domain was quantified by fluorescence at 448 nm. Binding curves
568 were fitted with a one-site binding model.

569

570 **Vps34-Sgk3 coupled kinase assay**

571 To monitor PI3P production by Vps34 and Crosstide phosphorylation by Sgk3 in a
572 single reaction, the components were mixed at following concentrations: 50 nM
573 Vps34 complex, 50 nM Sgk3, 500 μM Biotin-Crosstide, 0.5 mM ATP (spiked 1:10 with
574 γ^{32}P-ATP), 0.5 mM $MgCl_2$, 2 mM $MnCl_2$, 1 mM EGTA, 10% liver PI liposomes. The
575 reaction was carried out at 25°C and gentle shaking. 15 μl samples were mixed with
576 5 μl 4x quench buffer (20 mM Tris pH 7.4, 150 mM NaCl, 10 mM EDTA, 10 mM EGTA,
577 1% glycerol, 1 mM TCEP) at indicated time points. The quenched reactions were spun
578 for 5 min at 20800 g/20°C. The supernatant was mixed 1:1 with NeutrAvidin (Thermo
579 Scientific) at 2 mg/ml in water to sequester the biotinylated Crosstide and 5 ul were
580 spotted onto 0.45 um nitrocellulose membrane. The membrane was washed 5x3 min
581 with TBS (20 mM Tris pH 7.6, 137 mM NaCl), briefly dried, exposed in storage
582 phosphor screen overnight and imaged with an Amersham Typhoon
583 phosphorimager. The intensity of the spots was quantified in ImageJ. The pellets

584 containing liposomes with PI3^{32}P were washed 4 times with wash buffer (20 mM Tris
585 pH 7.4, 150 mM NaCl, 2.5 mM EDTA, 2.5 mM EGTA, 1% glycerol, 1 mM TCEP),
586 transferred into PCR tube and inserted into 20 ml polyethylene scintillation vials
587 containing 5 ml MilliQ water. PI3P synthesis was measured by liquid scintillation.

588

589 **HDX-MS**

590 *Lipid Vesicle Preparation*

591 Lipid films containing 20% cholesterol, 25% DOPC, 15% DOPS, 35% DOPE, and 5%
592 PI3P were dried and stored under argon for shipping. The dried films were
593 resuspended to 5 mM in gel filtration buffer (20 mM Tris pH 7.4, 150 mM NaCl, 1%
594 glycerol, 1 mM TCEP) by vortexing. The resuspended lipid vesicle solutions were
595 sonicated for 10 minutes, subjected to ten freeze-thaw cycles, and sonicated again for
596 5 minutes. The vesicles were then snap-frozen in liquid nitrogen and stored at -80°C

597 *HDX-MS sample preparation*

598 HDX reactions were conducted in a final reaction volume of 25 µL with a final Sgk3
599 concentration of 13 µM (for both FL and PX Sgk3). Prior to the addition of deuterated
600 solvent, 1.5 µL of FL or PX Sgk3 was allowed to incubate with either 2 µL of 5 mM 0%
601 PI3P vesicles or 2 µL 5 mM 5% PI3P vesciles. After the two minute incubation period,
602 21.5 µL D2O buffer (20mM pH 7 HEPES, 100mM NaCl, 0.5 mM TCEP, 94% D2O) was
603 added with a final %D2O of 81.5% (v/v). The reaction was allowed to proceed for 3s,
604 30s, 300s, or 3000s at 18°C before being quenched with ice cold acidic quench buffer.

605 All conditions and timepoints were created and run in triplicate. Samples were flash
606 frozen in liquid nitrogen and stored at -80°C until injection onto the ultra-
607 performance liquid chromatography system for proteolytic cleavage, peptide
608 separation, and injection onto a QTOF for mass analysis.

609 *Protein digestion and MS/MS data collection*

610 Protein samples were rapidly thawed and injected onto an integrated fluidics system
611 containing a HDx-3 PAL liquid handling robot and climate-controlled
612 chromatography system (LEAP Technologies), a Dionex Ultimate 3000 UHPLC
613 system, as well as an Impact HD QTOF Mass spectrometer (Bruker). The protein was
614 run over either one immobilized pepsin column at at 10°C (Trajan; ProDx protease
615 column, 2.1 mm x 30 mm PDX.PP01-F32) at 200 mL/min for 3 minutes. The resulting
616 peptides were collected and desalted on a C18 trap column (Acquity UPLC BEH C18
617 1.7mm column (2.1 x 5 mm); Waters 186003975). The trap was subsequently eluted
618 in line with a C18 reverse-phase separation column (Acquity 1.7 mm particle, 100 x 1
619 mm^2 C18 UPLC column, Waters 186002352), using a gradient of 5-36% B (Buffer A
620 0.1% formic acid; Buffer B 100% acetonitrile) over 16 minutes. Mass spectrometry
621 experiments acquired over a mass range from 150 to 2200 m/z using an electrospray
622 ionization source operated at a temperature of 200C and a spray voltage of 4.5 kV.

623 *Peptide identification*

624 Peptides were identified from the non-deuterated samples of FL and PX Sgk3 using
625 data-dependent acquisition following tandem MS/MS experiments (0.5 s precursor
626 scan from 150-2000 m/z; twelve 0.25 s fragment scans from 150-2000 m/z). MS/MS

627 datasets were analysed using PEAKS7 (PEAKS), and peptide identification was
628 carried out by using a false discovery based approach, with a threshold set to 1%
629 using a database of purified proteins and known contaminants found in Sf9 cells
630 (Dobbs *et al*, 2020). The search parameters were set with a precursor tolerance of 20
631 ppm, fragment mass error 0.02 Da, charge states from 1-8, leading to a selection
632 criterion of peptides that had a -10logP score of 21.4.

633 *Mass Analysis of Peptide Centroids and Measurement of Deuterium Incorporation*

634 HD-Examiner Software (Sierra Analytics) was used to automatically calculate the
635 level of deuterium incorporation into each peptide. All peptides were manually
636 inspected for correct charge state, correct retention time, appropriate selection of
637 isotopic distribution, etc. Deuteration levels were calculated using the centroid of the
638 experimental isotope clusters. Results are presented as relative levels of deuterium
639 incorporation and the only control for back exchange was the level of deuterium
640 present in the buffer (81.5%). Differences in exchange in a peptide were considered
641 significant if they met all three of the following criteria: : ≥7% change in exchange,
642 ≥0.5 Da difference in exchange, and a p value <0.01 using a two tailed student t-test.
643 All compared samples were set within the same experiment. To allow for
644 visualization of differences across all peptides, we utilized number of deuteron
645 difference (#D) plots. These plots show the total difference in deuterium
646 incorporation over the entire H/D exchange time course, with each point indicating a
647 single peptide. The mass spectrometry proteomics data have been deposited to the
648 ProteomeXchange Consortium via the PRIDE partner repository (Perez-Riverol *et al*,

649 2019) with the dataset identifier PXD025327. The data analysis statistics for all HDX-
650 MS experiments are in Supplementary Table 1 according to the guidelines of Masson
651 et al (Masson *et al*, 2019).

652

653 **References**

654

655 Alessi DR, Deak M, Casamayor A, Caudwell FB, Morrice N, Norman DG, Gaffney P,
656 Reese CB, MacDougall CN, Harbison D, *et al* (1997) 3-Phosphoinositide-
657 dependent protein kinase-1 (PDK1): structural and functional homology with
658 the Drosophila DSTPK61 kinase. *Curr Biol* 7: 776–89

659 Backer JM (2008) The regulation and function of Class III PI3Ks: novel roles for
660 Vps34. *Biochem J* 410: 1–17

661 Backer JM (2016) The intricate regulation and complex functions of the Class III
662 phosphoinositide 3-kinase Vps34. *Biochem J* 473: 2251–2271

663 Bago R, Malik N, Munson MJ, Prescott AR, Davies P, Sommer E, Shpiro N, Ward R,
664 Cross D, Ganley IG, *et al* (2014) Characterization of VPS34-IN1, a selective
665 inhibitor of Vps34, reveals that the phosphatidylinositol 3-phosphate-binding
666 SGK3 protein kinase is a downstream target of class III phosphoinositide 3-
667 kinase. *Biochem J* 463: 413–27

668 Bago R, Sommer E, Castel P, Crafter C, Bailey FP, Shpiro N, Baselga J, Cross D, Eyers
669 PA & Alessi DR (2016) The hVps34-SGK3 pathway alleviates sustained
670 PI3K/Akt inhibition by stimulating mTORC1 and tumour growth. *EMBO J* 35:
671 1902–22

672 Braccini L, Ciraolo E, Campa CC, Perino A, Longo DL, Tibolla G, Pregnolato M, Cao Y,
673 Tassone B, Damilano F, *et al* (2015) PI3K-C2γ is a Rab5 effector selectively

674 controlling endosomal Akt2 activation downstream of insulin signalling. *Nat*
675 *Commun* 6: 7400

676 Brunet A, Park J, Tran H, Hu LS, Hemmings BA & Greenberg ME (2001) Protein
677 kinase SGK mediates survival signals by phosphorylating the forkhead
678 transcription factor FKHRL1 (FOXO3a). *Mol Cell Biol* 21: 952–65

679 Carlton JG & Cullen PJ (2005) Coincidence detection in phosphoinositide signaling.
680 *Trends Cell Biol* 15: 540–547

681 Chan TO, Zhang J, Rodeck U, Pascal JM, Armen RS, Spring M, Dumitru CD, Myers V, Li
682 X, Cheung JY, *et al* (2011) Resistance of Akt kinases to dephosphorylation
683 through ATP-dependent conformational plasticity. *Proc Natl Acad Sci U S A* 108:
684 E1120-7

685 Chandra M, Chin YK-Y, Mas C, Feathers JR, Paul B, Datta S, Chen K-E, Jia X, Yang Z,
686 Norwood SJ, *et al* (2019) Classification of the human phox homology (PX)
687 domains based on their phosphoinositide binding specificities. *Nat Commun* 10:
688 1528

689 Chen W, Chen Y, Xu B, Juang Y-C, Stippec S, Zhao Y & Cobb MH (2009) Regulation of
690 a third conserved phosphorylation site in SGK1. *J Biol Chem* 284: 3453–60

691 Cox J & Mann M (2008) MaxQuant enables high peptide identification rates,
692 individualized p.p.b.-range mass accuracies and proteome-wide protein
693 quantification. *Nat Biotechnol* 26: 1367–72

694 Currie RA, Walker KS, Gray A, Deak M, Casamayor A, Downes CP, Cohen P, Alessi DR

695 & Lucocq J (1999) Role of phosphatidylinositol 3,4,5-trisphosphate in
696 regulating the activity and localization of 3-phosphoinositide-dependent
697 protein kinase-1. *Biochem J* 337 (Pt 3: 575–83

698 Dai F, Yu L, He H, Chen Y, Yu J, Yang Y, Xu Y, Ling W & Zhao S Human serum and
699 glucocorticoid-inducible kinase-like kinase (SGKL) phosphorylates glycogen
700 syntheses kinase 3 beta (GSK-3b) at serine-9 through direct interaction

701 Dobbs JM, Jenkins ML & Burke JE (2020) Escherichia coli and Sf9 Contaminant
702 Databases to Increase Efficiency of Tandem Mass Spectrometry Peptide
703 Identification in Structural Mass Spectrometry Experiments. *J Am Soc Mass*
704 *Spectrom* 31: 2202–2209

705 Ebner M, Lučić I, Leonard TA & Yudushkin I (2017) PI(3,4,5)P3 Engagement
706 Restricts Akt Activity to Cellular Membranes. *Mol Cell* 65: 416-431.e6

707 Elsner DJ, Siess KM, Gossenreiter T, Hartl M & Leonard TA (2019) A ubiquitin-like
708 domain controls protein kinase D dimerization and activation by trans-
709 autophosphorylation. *J Biol Chem* 294: 14422–14441

710 Endicott JA, Noble MEM & Johnson LN (2012) The structural basis for control of
711 eukaryotic protein kinases. *Annu Rev Biochem* 81: 587–613

712 Facchinetti V, Ouyang W, Wei H, Soto N, Lazorchak A, Gould C, Lowry C, Newton AC,
713 Mao Y, Miao RQ, *et al* (2008) The mammalian target of rapamycin complex 2
714 controls folding and stability of Akt and protein kinase C. *EMBO J* 27: 1932–43

715 Fruman DA, Chiu H, Hopkins BD, Bagrodia S, Cantley LC & Abraham RT (2017) The

716 PI3K Pathway in Human Disease. *Cell* 170: 605–635

717 Fruman DA & Rommel C (2014) PI3K and cancer: lessons, challenges and
718 opportunities. *Nat Rev Drug Discov* 13: 140–156

719 Gasser JA, Inuzuka H, Lau AW, Wei W, Beroukhim R & Toker A (2014) SGK3
720 mediates INPP4B-dependent PI3K signaling in breast cancer. *Mol Cell* 56: 595–
721 607

722 Goulden BD, Pacheco J, Dull A, Zewe JP, Deiters A & Hammond GR V (2019) A high-
723 avidity biosensor reveals plasma membrane PI(3,4)P2 is predominantly a class
724 I PI3K signaling product. *J Cell Biol* 218: 1066–1079

725 Hastie CJ, McLauchlan HJ & Cohen P (2006) Assay of protein kinases using
726 radiolabeled ATP: A protocol. *Nat Protoc* 1: 968–971

727 Hauge C, Antal TL, Hirschberg D, Doehn U, Thorup K, Idrissova L, Hansen K, Jensen
728 ON, Jørgensen TJ, Biondi RM, *et al* (2007) Mechanism for activation of the
729 growth factor-activated AGC kinases by turn motif phosphorylation. *EMBO J* 26:
730 2251–2261

731 Hornbeck P V., Chabra I, Kornhauser JM, Skrzypek E & Zhang B (2004) PhosphoSite:
732 A bioinformatics resource dedicated to physiological protein phosphorylation.
733 *Proteomics* 4: 1551–61

734 Hurley JH & Young LN (2017) Mechanisms of Autophagy Initiation. *Annu Rev*
735 *Biochem* 86: 225–244

736 Ikenoue T, Inoki K, Yang Q, Zhou X & Guan K-L (2008) Essential function of TORC2 in

737 PKC and Akt turn motif phosphorylation, maturation and signalling. *EMBO J* 27:
738 1919–1931

739 Ivetac I, Munday AD, Kisseleva M V., Zhang X-M, Luff S, Tiganis T, Whisstock JC, Rowe
740 T, Majerus PW & Mitchell CA (2005) The type Ialpha inositol polyphosphate 4-
741 phosphatase generates and terminates phosphoinositide 3-kinase signals on
742 endosomes and the plasma membrane. *Mol Biol Cell* 16: 2218–33

743 Kobayashi T & Cohen P (1999) Activation of serum- and glucocorticoid-regulated
744 protein kinase by agonists that activate phosphatidylinositide 3-kinase is
745 mediated by 3-phosphoinositide-dependent protein kinase-1 (PDK1) and
746 PDK2. *Biochem J* 339 (Pt 2: 319–28

747 Kobayashi T, Deak M, Morrice N & Cohen P (1999) Characterization of the structure
748 and regulation of two novel isoforms of serum- and glucocorticoid-induced
749 protein kinase. *Biochem J* 344 Pt 1: 189–97

750 Landel I, Quambusch L, Depta L & Rauh D (2020) Spotlight on AKT: Current
751 Therapeutic Challenges. *ACS Med Chem Lett* 11: 225–227

752 Lang F, Bohmer C, Palmada M, Seebohm G, Strutz-Seebohm N & Vallon V (2006)
753 (Patho)physiological Significance of the Serum- and Glucocorticoid-Inducible
754 Kinase Isoforms. *Physiol Rev* 86: 1151–1178

755 Lapierre J-M, Eathiraj S, Vensel D, Liu Y, Bull CO, Cornell-Kennon S, Iimura S,
756 Kelleher EW, Kizer DE, Koerner S, *et al* (2016) Discovery of 3-(3-(4-(1-
757 Aminocyclobutyl)phenyl)-5-phenyl-3H-imidazo[4,5-b]pyridin-2-yl)pyridin-2-

758 amine (ARQ 092): An Orally Bioavailable, Selective, and Potent Allosteric AKT
759 Inhibitor. *J Med Chem* 59: 6455–69

760 Leonard TA & Hurley JH (2011) Regulation of protein kinases by lipids. *Curr Opin*
761 *Struct Biol* 21: 785–791

762 Leonard TA, Róycki B, Saidi LF, Hummer G & Hurley JH (2011) Crystal structure and
763 allosteric activation of protein kinase C βiI. *Cell* 144: 55–66

764 Lin K, Lin J, Wu W-I, Ballard J, Lee BB, Gloor SL, Vigers GPA, Morales TH, Friedman
765 LS, Skelton N, *et al* (2012) An ATP-site on-off switch that restricts phosphatase
766 accessibility of Akt. *Sci Signal* 5: ra37

767 Liu D, Yang X & Songyang Z (2000) Identification of CISK, a new member of the SGK
768 kinase family that promotes IL-3-dependent survival. *Curr Biol* 10: 1233–6

769 Liu S-L, Wang Z-G, Hu Y, Xin Y, Singaram I, Gorai S, Zhou X, Shim Y, Min J-H, Gong L-
770 W, *et al* (2018) Quantitative Lipid Imaging Reveals a New Signaling Function of
771 Phosphatidylinositol-3,4-Bisphophate: Isoform- and Site-Specific Activation of
772 Akt. *Mol Cell* 71: 1092-1104.e5

773 Lu S, Deng R, Jiang H, Song H, Li S, Shen Q, Huang W, Nussinov R, Yu J & Zhang J
774 (2015) The Mechanism of ATP-Dependent Allosteric Protection of Akt Kinase
775 Phosphorylation. *Structure* 23: 1725–1734

776 Lučić I, Rathinaswamy MK, Truebestein L, Hamelin DJ, Burke JE & Leonard TA
777 (2018) Conformational sampling of membranes by Akt controls its activation
778 and inactivation. *Proc Natl Acad Sci U S A* 115: E3940–E3949

779 Lučić I, Truebestein L & Leonard TA (2016) Novel Features of DAG-Activated PKC
780 Isozymes Reveal a Conserved 3-D Architecture. *J Mol Biol* 428: 121–141

781 Malik N, Macartney T, Hornberger A, Anderson KE, Tovell H, Prescott AR & Alessi DR
782 (2018) Mechanism of activation of SGK3 by growth factors via the Class 1 and
783 Class 3 PI3Ks. *Biochem J* 475: 117–135

784 Malik N, Nirujogi RS, Peltier J, Macartney T, Wightman M, Prescott AR, Gourlay R,
785 Trost M, Alessi DR & Karapetsas A (2019) Phosphoproteomics reveals that the
786 hVPS34 regulated SGK3 kinase specifically phosphorylates endosomal proteins
787 including Syntaxin-7, Syntaxin-12, RFIP4 and WDR44. *Biochem J* 476: 3081–
788 3107

789 Manning G (2002) The Protein Kinase Complement of the Human Genome. *Science*
790 *(80-)* 298: 1912–1934

791 Marone R, Cmiljanovic V, Giese B & Wymann MP (2008) Targeting phosphoinositide
792 3-kinase-Moving towards therapy. *Biochim Biophys Acta - Proteins Proteomics*
793 1784: 159–185 doi:10.1016/j.bbapap.2007.10.003 [PREPRINT]

794 Martini M, De Santis MC, Braccini L, Gulluni F & Hirsch E (2014) PI3K/AKT signaling
795 pathway and cancer: an updated review. *Ann Med* 46: 372–383

796 Masson GR, Burke JE, Ahn NG, Anand GS, Borchers C, Brier S, Bou-Assaf GM, Engen
797 JR, Englander SW, Faber J, *et al* (2019) Recommendations for performing,
798 interpreting and reporting hydrogen deuterium exchange mass spectrometry
799 (HDX-MS) experiments. *Nat Methods* 16: 595–602

800 Murray JT, Cummings LA, Bloomberg GB & Cohen P (2005) Identification of different
801 specificity requirements between SGK1 and PKBα. *FEBS Lett* 579: 991–994

802 Oancea E & Meyer T (1998) Protein kinase C as a molecular machine for decoding
803 calcium and diacylglycerol signals. *Cell* 95: 307–18

804 Oh WJ, Wu C, Kim SJ, Facchinetti V, Julien L-A, Finlan M, Roux PP, Su B & Jacinto E
805 (2010) mTORC2 can associate with ribosomes to promote cotranslational
806 phosphorylation and stability of nascent Akt polypeptide. *EMBO J* 29: 3939–
807 3951

808 Pao AC, McCormick JA, Li H, Siu J, Govaerts C, Bhalla V, Soundararajan R & Pearce D
809 (2007) NH 2 terminus of serum and glucocorticoid-regulated kinase 1 binds to
810 phosphoinositides and is essential for isoform-specific physiological functions.
811 *Am J Physiol Physiol* 292: F1741–F1750

812 Perez-Riverol Y, Csordas A, Bai J, Bernal-Llinares M, Hewapathirana S, Kundu DJ,
813 Inuganti A, Griss J, Mayer G, Eisenacher M, *et al* (2019) The PRIDE database and
814 related tools and resources in 2019: improving support for quantification data.
815 *Nucleic Acids Res* 47: D442–D450

816 Rappsilber J, Mann M & Ishihama Y (2007) Protocol for micro-purification,
817 enrichment, pre-fractionation and storage of peptides for proteomics using
818 StageTips. *Nat Protoc* 2: 1896–906

819 Sawa-Makarska J, Baumann V, Coudevylle N, von Bülow S, Nogellova V, Abert C,
820 Schuschnig M, Graef M, Hummer G & Martens S (2020) Reconstitution of

821 autophagosome nucleation defines Atg9 vesicles as seeds for membrane
822 formation. *Science* 369

823 Schenck A, Goto-Silva L, Collinet C, Rhinn M, Giner A, Habermann B, Brand M &
824 Zerial M (2008) The endosomal protein Appl1 mediates Akt substrate
825 specificity and cell survival in vertebrate development. *Cell* 133: 486–97

826 Siess KM & Leonard TA (2019) Lipid-dependent Akt-ivity: where, when, and how.
827 *Biochem Soc Trans* 47: 897–908

828 Slagsvold T, Marchese A, Brech A & Stenmark H (2006) CISK attenuates degradation
829 of the chemokine receptor CXCR4 via the ubiquitin ligase AIP4. *EMBO J* 25:
830 3738–49

831 Song Y, DiMaio F, Yu-Ruei Wang R, Kim D, Miles C, Brunette T, Thompson J & Baker
832 D Technical Advance High-Resolution Comparative Modeling with RosettaCM.

833 Stokoe D, Stephens LR, Copeland T, Gaffney PR, Reese CB, Painter GF, Holmes AB,
834 McCormick F & Hawkins PT (1997) Dual role of phosphatidylinositol-3,4,5-
835 trisphosphate in the activation of protein kinase B. *Science* 277: 567–70

836 Tessier M & Woodgett JR (2006) Role of the Phox homology domain and
837 phosphorylation in activation of serum and glucocorticoid-regulated kinase-3. *J*
838 *Biol Chem* 281: 23978–89

839 Theile CS, Witte MD, Blom AEM, Kundrat L, Ploegh HL & Guimaraes CP (2013) Site-
840 specific N-terminal labeling of proteins using sortase-mediated reactions. *Nat*
841 *Protoc* 8: 1800–1807

842 Tovell H, Testa A, Zhou H, Shpiro N, Crafter C, Ciulli A & Alessi DR (2019) Design and
843 Characterization of SGK3-PROTAC1, an Isoform Specific SGK3 Kinase PROTAC
844 Degrader. *ACS Chem Biol*: acschembio.9b00505

845 Vasudevan KM, Barbie DA, Davies MA, Rabinovsky R, McNear CJ, Kim JJ, Hennessy
846 BT, Tseng H, Pochanard P, Kim SY, *et al* (2009) AKT-independent signaling
847 downstream of oncogenic PIK3CA mutations in human cancer. *Cancer Cell* 16:
848 21–32

849 Virbasius J V, Song X, Pomerleau DP, Zhan Y, Zhou GW & Czech MP (2001) Activation
850 of the Akt-related cytokine-independent survival kinase requires interaction of
851 its phox domain with endosomal phosphatidylinositol 3-phosphate. *Proc Natl*
852 *Acad Sci U S A* 98: 12908–13

853 Wang Y, Zhou D, Phung S, Warden C, Rashid R, Chan N & Chen S (2017) SGK3
854 sustains ERα signaling and drives acquired aromatase inhibitor resistance
855 through maintaining endoplasmic reticulum homeostasis. *Proc Natl Acad Sci U S*
856 *A* 114: E1500–E1508

857 Webster MK, Goya L, Ge Y, Maiyar AC & Firestone GL (1993) Characterization of sgk,
858 a novel member of the serine/threonine protein kinase gene family which is
859 transcriptionally induced by glucocorticoids and serum. *Mol Cell Biol* 13: 2031–
860 2040

861 Weisner J, Landel I, Reintjes C, Uhlenbrock N, Trajkovic-Arsic M, Dienstbier N,
862 Hardick J, Ladigan S, Lindemann M, Smith S, *et al* (2019) Preclinical Efficacy of
863 Covalent-Allosteric AKT Inhibitor Borussertib in Combination with Trametinib

864 in KRAS-mutant Pancreatic and Colorectal Cancer. *Cancer Res* 79:
865 canres.2861.2018

866 Wu W-I, Voegtli WC, Sturgis HL, Dizon FP, Vigers GPA & Brandhuber BJ (2010)
867 Crystal structure of human AKT1 with an allosteric inhibitor reveals a new
868 mode of kinase inhibition. *PLoS One* 5: e12913

869 Xing Y, Liu D, Zhang R, Joachimiak A, Songyang Z & Xu W (2004) Structural basis of
870 membrane targeting by the Phox homology domain of cytokine-independent
871 survival kinase (CISK-PX). *J Biol Chem* 279: 30662–9

872 Xu J, Liu D, Gill G & Songyang Z (2001) Regulation of cytokine-independent survival
873 kinase (CISK) by the phox homology domain and phosphoinositides. *J Cell Biol*
874 154: 699–705

875

876

877 **Figure 1. Sgk3 localizes specifically to PI3P-containing endosomes**

878 **A)** HeLa cells were transfected with mCherry-Sgk3^{WT} and serum starved
879 overnight.

880 **B)** Starved cells were treated with 100 nM wortmannin for 20 min.

881 **C-E)** Cells were co-transfected with mCherry-Sgk3^{WT} and EGFP-Sgk3^{R90A} mutant.

882 **F)** Fluorescence intensity profile of mCherry Sgk3^{WT} and EGFP-Sgk3^{R90A} along the
883 white line shown in C-E.

884

885 **Figure 2. Sgk3 is specifically and allosterically activated by PI3P**

886 **A)** Sgk3^{WT} kinase activity was assayed in the presence (closed black square) or
887 absence (closed red square) of 100 μM Crosstide substrate with 0-4 mol %
888 PI3P liposomes, or with 4 mol % PI(4,5)P_2 liposomes (open black square) as a
889 negative control. In parallel, binding of Sgk3 to 0-4 % PI3P liposomes (full blue
890 circles) or 4% PI(4,5)P_2 (open blue circle) as a negative control was measured.
891 Dotted black line indicates basal Sgk3^{WT} kinase activity of unbound protein,
892 dotted red line indicates no-substrate control. Kinase activity was read out
893 radiometrically by liquid scintillation and liposome binding by Coomassie
894 densitometry. Error bars are the standard deviation of three independent
895 experiments.

896 **B)** Same as A) with Sgk3^{D286A} kinase-dead mutant.

897 **C)** Schematic of Vps34-Sgk3 coupled kinase assay. Phosphorylation of Crosstide
898 was assayed by phosphorimaging. PI3P synthesis was measured by liquid
899 scintillation.
900 **D)** Vps34-Sgk3 coupled kinase assay. Crosstide phosphorylation was measured
901 in the presence (full blue line) or absence (dashed blue line) of 50 nM Vps34.
902 At the same time, PI3P synthesis was measured in the presence (full green
903 line) or absence (dashed green line) of 50 nM Vps34. Error bars are the
904 standard deviation of three independent experiments.

905

906 **Figure 3. Sgk3 is autoinhibited by its PX domain.**

907 **A)** Comparison of deuterium incorporation in Sgk3 PX domain with 0% vs 5%
908 PI3P liposomes. Plot: difference in number of deuterons incorporated as a
909 function of peptide centroid over the PX domain. Negative numbers indicate
910 protection (blue). Peptides showing significant deuterium exchange
911 differences (>7%, >0.5 Da, and $p<0.01$) were mapped on the structure of the
912 human Sgk3 PX domain (PDB:6EDX). The binding site for PI3P is indicated by
913 superimposing the structure of the PX domain of p40phox in complex with
914 PI3P (PDB: 1H6H) and rendering the PI3P in spheres.
915 **B)** Comparison of deuterium incorporation in $Sgk3^{WT}$ vs. Sgk3 PX domain in the
916 presence of 0% PI3P liposomes (unbound). Plot: difference in number of
917 deuterons incorporated as a function of peptide centroid over the PX domain.
918 Positive numbers indicate domain exposure (red).

919 **C)** Comparison of deuterium incorporation in Sgk3^{WT} unbound (0% PI3P) vs
920 bound (5% PI3P) for the PX domain (left) and the kinase domain (right). A
921 homology model of Sgk3 kinase domain (Rosetta) (Song *et al*) was used to map
922 the changes. Color coding expressing the magnitude of changes in deuterium
923 incorporation is on bottom right. All measurements were done in triplicates,
924 error bars are the standard deviations.

925

926 **Figure 4. Autoinhibition of Sgk3 impairs binding to PI3P**

927 **A)** Binding of Sgk3^{WT} full-length (blue squares) and FITC-labelled Sgk3 PX
928 domain (black squares) to 0-4 mol % PI3P liposomes was monitored in single
929 reaction using fluorescence (FITX-PX) or Coomassie densitometry (full-length
930 Sgk3) in 15% SDS-PAGE gels. Curves were fitted with a one binding site model.
931 Error bars are the standard deviations of three independent experiments.

932 **B-D)** Distribution of EGFP-PX domain (B) or mCherry-Sgk3^{WT} (full-length) (C) in
933 serum-starved HeLa cells.

934 **E)** Quantification of fluorescence intensity of both constructs along the white line
935 shown in images B-D.

936

937 **Figure 5. Model for the allosteric activation of Sgk3 by PI3P**

938 Cytosolic Sgk3 is allosterically inhibited by its PX domain, which is relieved by
939 PI3P binding (1). This is followed by phosphorylation of the Sgk3 activation loop

940 by PDK1 as a consequence of its association with endosomal PI(3,4)P_2 (2).
941 Phosphorylation activates Sgk3 (3), thereby permitting downstream substrate
942 phosphorylation (4).

943

944

Figure 1. Sgk3 localizes specifically to PI3P-containing endosomes.

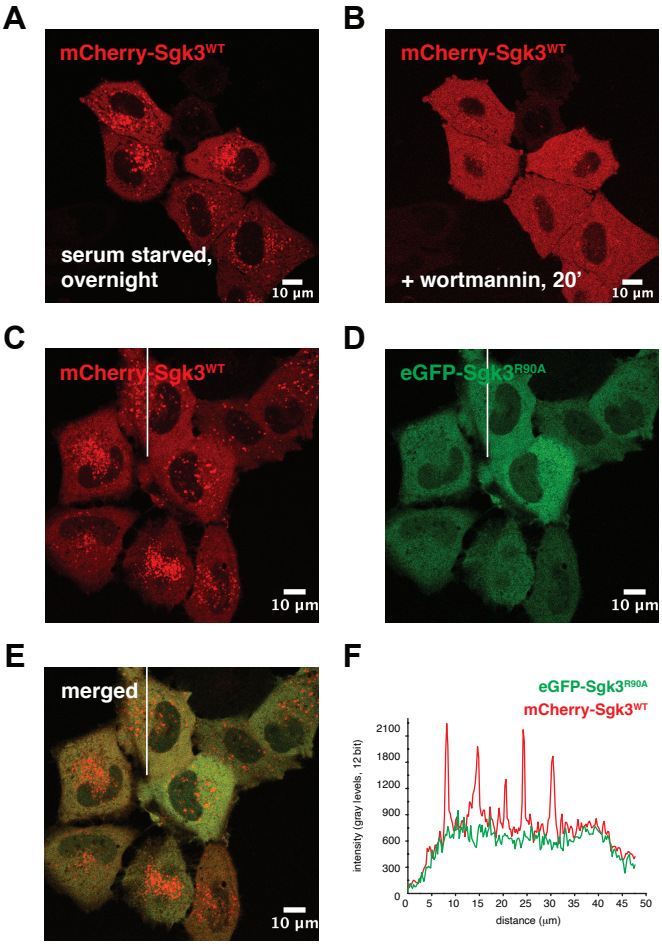

Figure 2. Sgk3 is specifically and allosterically activated by PI3P.

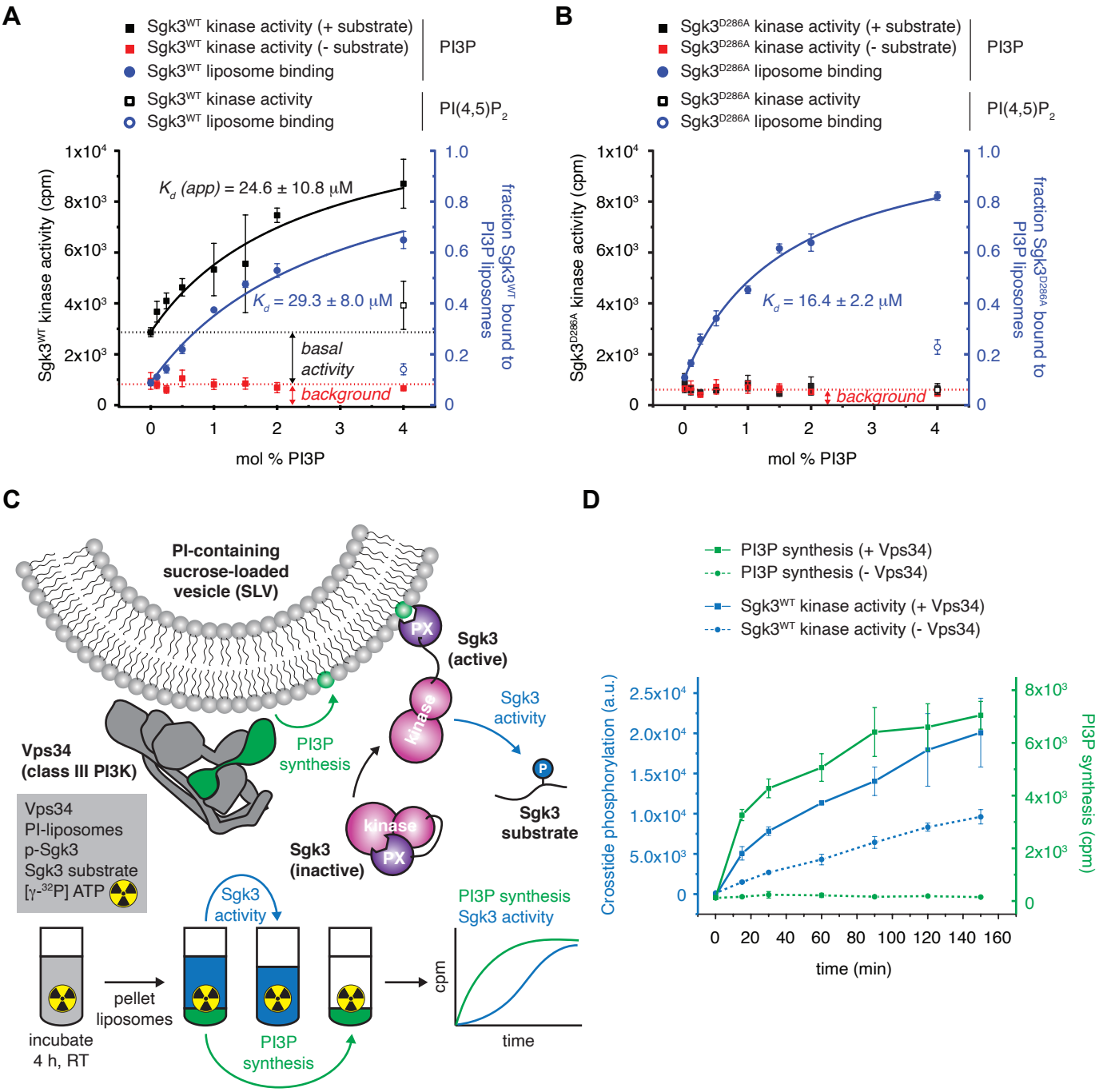

Figure 3. Sgk3 is autoinhibited by its PX domain.

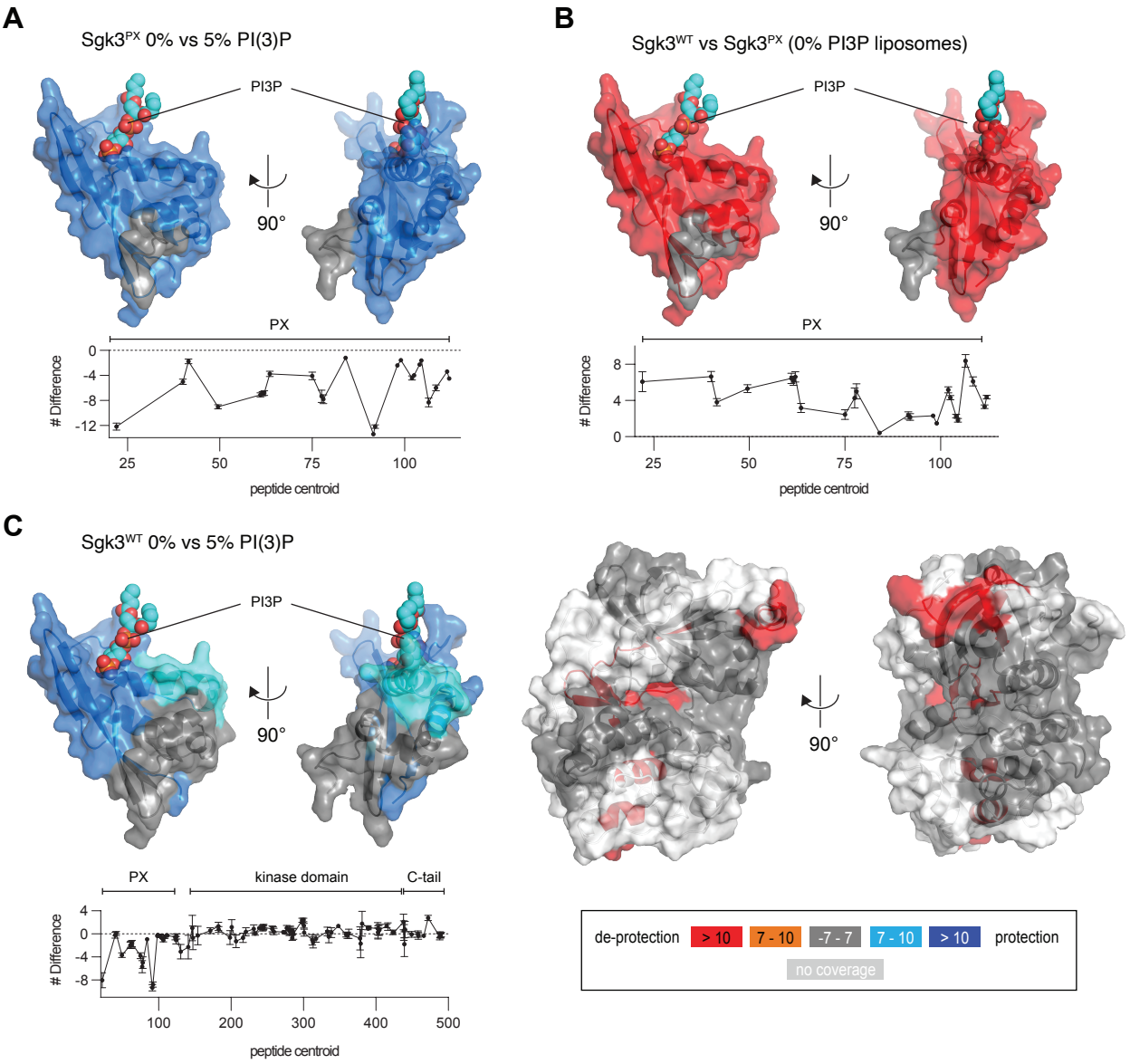

Figure 4. Autoinhibition of Sgk3 impairs binding to PI3P.

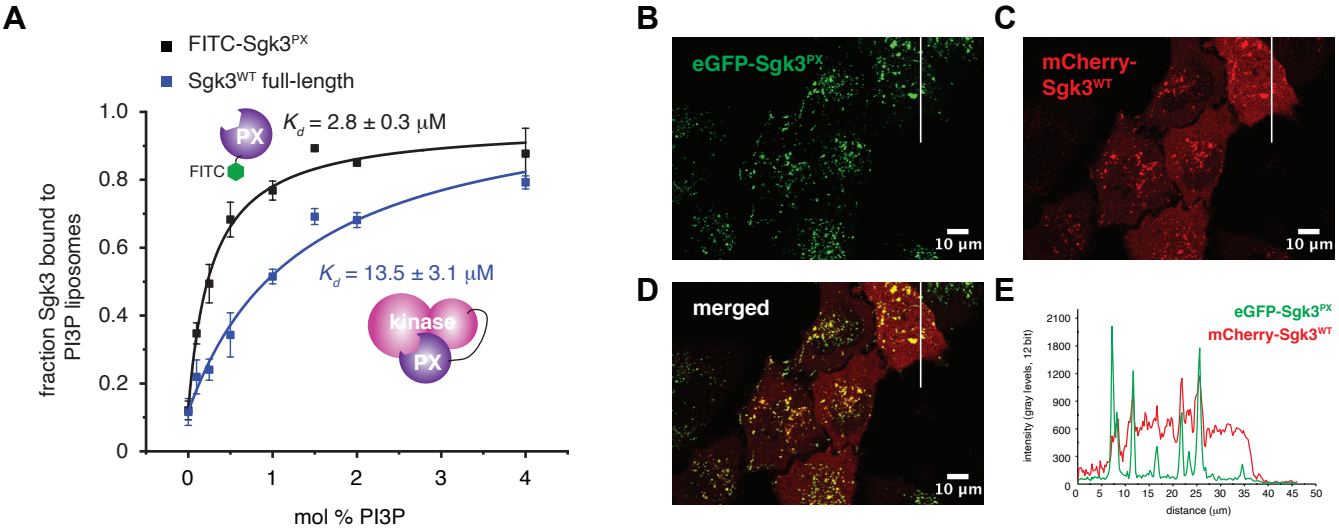
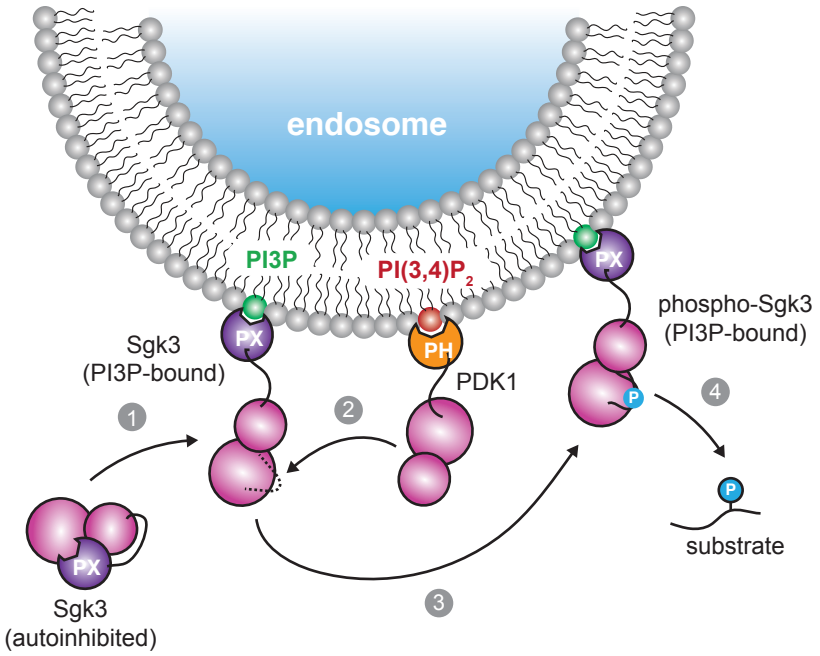
Figure 5. Model for the allosteric activation of Sgk3 by PI3P.